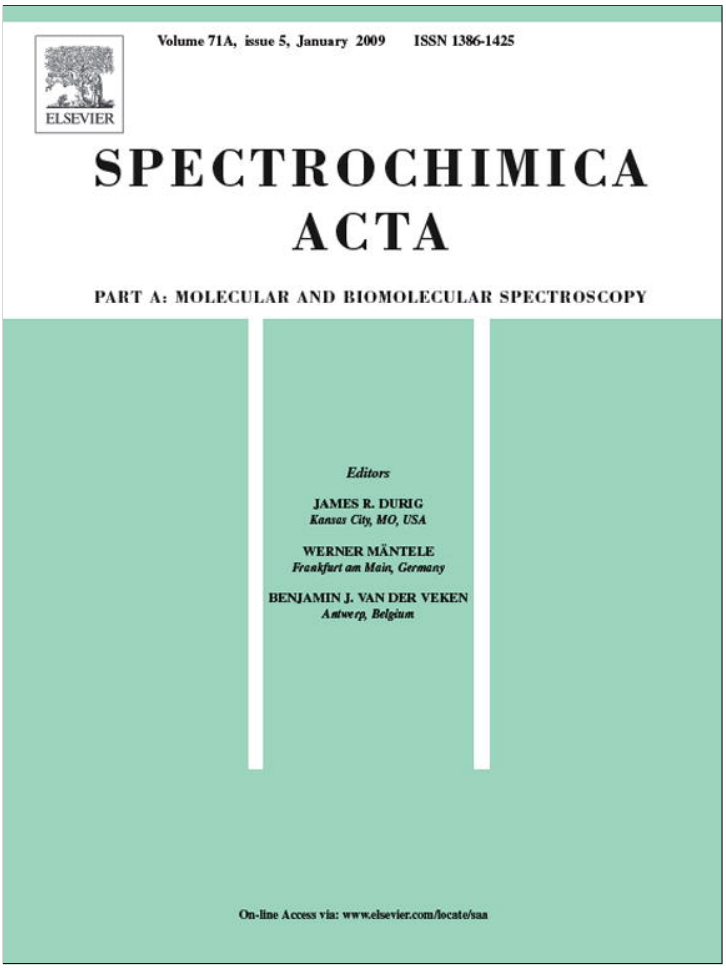

Spectrochimica Acta Part A 71 (2009) 1989–1998

Contents lists available at ScienceDirect

Spectrochimica Acta Part A: Molecular and Biomolecular Spectroscopy

journal homepage: www.elsevier.com/locate/saa

Spectroscopic and theoretical study of 2-acetylphenyl-2-naphthoate

Gabriel S. Suarez[a], Néstor E. Massa[b], Alicia H. Jubert[c,*], Jorge L. Jios[d], Juan C. Autino[e], Gustavo P. Romanelli[e,f]

[a] Departamento de Ingeniería Química, Facultad de Ingeniería, Universidad Nacional de La Plata, 1900 La Plata, Argentina
[b] Laboratorio Nacional de Investigación y Servicios en Espectroscopia Óptica-Centro CEQUINOR, Universidad Nacional de La Plata, CC 962, 1900 La Plata, Argentina
[c] CEQUINOR, Departamento de Química y Facultad de Ingeniería, Universidad Nacional de La Plata, 1900 La Plata, Argentina
[d] Laboratorio de Servicios para la Industria y el sistema Científico, LASEISIC, Departamento de Química, Universidad Nacional de La Plata, Camino Centenario entre 505 y 508, 1897 Gonnet, Argentina
[e] Laboratorio de Estudio de Compuestos Orgánicos (LADECOR), Departamento de Química, Universidad Nacional de La Plata, 1900 La Plata, Argentina
[f] Centro de Investigación y Desarrollo en Ciencias Aplicadas "Dr. Jorge Ronco" (CINDECA), Departamento de Química, Universidad Nacional de La Plata, 1900 La Plata, Argentina

ARTICLE INFO

Article history:
Received 5 February 2008
Accepted 21 July 2008

Keywords:
2-Acetylphenyl-2-naphthoate
IR
Raman
NMR
DFT

ABSTRACT

Mid-, far-infrared and Raman vibrational spectra of 2-acetylphenyl-2-naphthoate have been measured at room and low temperatures. The molecule was also analyzed by means of *ab initio* calculations. The conformational space has been scanned using molecular dynamics and complemented with functional density calculations that optimize the geometry of the lowest energy conformers 2-acetylphenyl-2-naphthoate as obtained in the simulations. The vibrational frequencies and the ^{1}H and ^{13}C NMR chemical shifts were assigned using functional density calculations. The theoretical chemical shift values were compared with the experimental ones. The molecular electrostatic potential maps were obtained and analyzed.

1. Introduction

The 2-acetylphenyl-2-naphthoate belongs to the family of 2-acylaryl arenecarboxylates, esters that are potential intermediates in the synthesis of several compounds possessing bioactivities of different types, such as antitumoral [1,2], antibacterial [3,4], antifungal [5,6] and pesticide [7,8]. Besides, acetylphenyl naphthoates are intermediates in the preparation of naphthylchromones as potential tanning agents [9,10].

The preparation of the title compound involves the condensation of 2′-hydroxyacetophenone(II), which can be obtained from phenol *via* Fries rearrangement, with 2-naphthoyl acid chloride in pyridine [9,10] (Scheme 1).

Previously, we have done in a series of 2-acetylaryl esters the conformational analysis by multinuclear (^{1}H, ^{13}C and ^{17}O) magnetic resonance spectroscopy [11] and developed a quantitative structure–retention relationships theory to compute chromatographic parameters [12].

There is no single crystal X-ray diffraction data of the 2-acetylphenyl-2-naphthoate, nevertheless the reported 2-acetylphenyl-1-naphthoate structure [13] is closely related to the title compound since it constitutes their constitutional isomer. The OC(O)– carbonyl carbon is bonded in this molecule to the carbon C1″ instead of the C2″ of the naphthalene ring (the numbering refers to those adopted in Fig. 1). This difference probably causes the variation of the torsion angle connecting both aromatic rings, but the bond lengths of all atoms and the bond angles and torsion angles of the aromatic rings are expected to keep approximately the same values in both isomers. Reported single crystal X-ray diffraction data of the 2-acetylphenyl-1-naphthoate [13] show that the molecule is not planar as consequence of the fusion of 1-naphthoic acid and acetophenone moieties: i.e., the torsion angle between the benzene and naphthalene ring planes is 77.39(7)°. Two intramolecular C–H···O bonds and a short intramolecular O···O distance of 2.719(2) Å have been observed for this unsubstituted compound [13].

Multinuclear (^{1}H, ^{13}C and ^{17}O) magnetic resonance spectroscopy was also used to study the behavior of various substituted 2-acetylphenyl-1- and 2-naphthoates in deuterochloroform (^{1}H and ^{13}C) and hot acetonitrile solution (^{17}O) [11]. ^{1}H RMN spectra have shown the following main features: (a) hydrogen atoms attached to the phenyl ring are not perturbed by the change in the orientation of the naphthyl group (1- or 2-naphthyl). (b) A *peri*-effect at H-8″ exists (Ref. [11], Scheme 1). (c) Hydrogen atoms

* Corresponding author. Tel.: +54 221 4 259485; fax: +54 221 4 259485.
E-mail address: jubert@quimica.unlp.edu.ar (A.H. Jubert).

1386-1425/$ – see front matter © 2008 Elsevier B.V. All rights reserved.
doi:10.1016/j.saa.2008.07.048

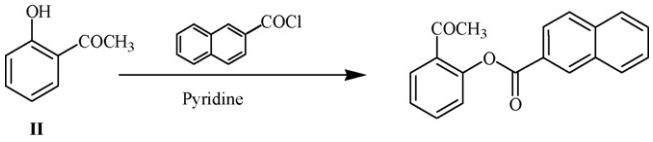

Scheme 1. Preparation procedure of the 2-acetylphenyl-2-naphthoate.

H-6″ and H-7″ reversed their chemical shift sequence according to the mesomeric effects in the corresponding naphthyl group. In turn, ^{17}O chemical shift values reflect very sensitively the electronic changes due to both conformation and substitution [14]. The oxygen atoms of the oxycarbonyl group in the 2-acetylphenyl-1- and 2-naphthoates have chemical shifts that strongly depend on their location to the naphthyl group [11]. Those of the carbonyl oxygen are about 20 ppm higher in the 1- than in the 2-series, and for the O–(CO) atom the difference is about 10 ppm, this is attributed to a steric perturbation in the 1-naphthyl compounds. Interestingly, these effects do not correlate with torsion angles, reflecting coplanarity of this moiety of the molecules.

Molecular electrostatic potential maps (MEPs) are useful in understanding sites for electrophilic attack [15]. The electrostatic potential $V(r)$ is good for studying processes based on the "recognition" of one molecule by another, as in drug–receptor, and enzyme–substrate interaction, because it is through their potentials that the two species first "see" each other [16,17]. Being a real physical property, $V(r)$s can be determined experimentally by diffraction or by computational methods [18].

In this manuscript we use the approach first proposed by Politzer et al. [19–22] for electrostatic potentials to predict and interpret nucleophilic processes [23].

The problem in calculating magnetic shielding within *ab initio* or density functional theory (DFT) had been solved [24,25], rapid progress was made in developing techniques such as gauge invariant (or including) atomic orbitals (GIAO) [26,27] or individual gauge for localized orbitals (IGLO) [28] that are able to calculate magnetic properties efficiently and quite accurately. Extensions of the original Hartree–Fock (HF) formalisms to second-order Møller–Plesset (MP2) [29] and DFT [30] calculations were used to improve the accuracy of the calculated values.

Determining chemical shifts for direct comparison with experimental spectra remains a major use of *ab initio* or DFT magnetic shielding calculations. Generally, chemical shifts on the δ-scale are calculated by taking the difference between the calculated shielding and that found for a reference molecule such as tetramethylsilane (TMS). However, as Chesnut [31] as well as Forsyth and Sebag [32] have pointed out, this is not the best procedure and better results can be obtained by setting up a linear regression equation between calculated shieldings and experimental chemical shifts. van Eikema Hommes and Clark [33] reported parameters for such regression equations for 18 calculation levels commonly used with the Gaussian series of programs [34] and gave root mean-square deviations for each level based on the training dataset.

We found that simple linear regression technique improves the accuracy of ^{13}C and ^{1}H chemical shifts for both, with DFT and *ab initio* methods. Chemical shifts calculated using the appropriate regression equation were then appropriate enough to allow assignment of spectral features and even identification, in many cases, of tautomers. Similar performance is found at the relatively inexpensive B3LYP/6-31G(d)//B3LYP/6-31G(d) level of theory to more computationally intensive methods.

In this work we report the experimental and theoretical studies of 2-acetylphenyl-2-naphthoate in an effort to contribute with a deeper insight on the physicochemical properties of this compound and a better knowledge of their chemical reactivity. In the following we discuss mid-, far-infrared, Raman and NMR spectra of 2-acetylphenyl-2-naphthoate at room and low temperatures assigning vibrational frequencies using functional density calculations. The conformational space of this molecule was scanned using molecular dynamics (MD) calculations and density calculations toward optimizing the geometry of the lowest energy conformers as obtained in the simulations. As pointed above the MEPs are obtained and analyzed [18].

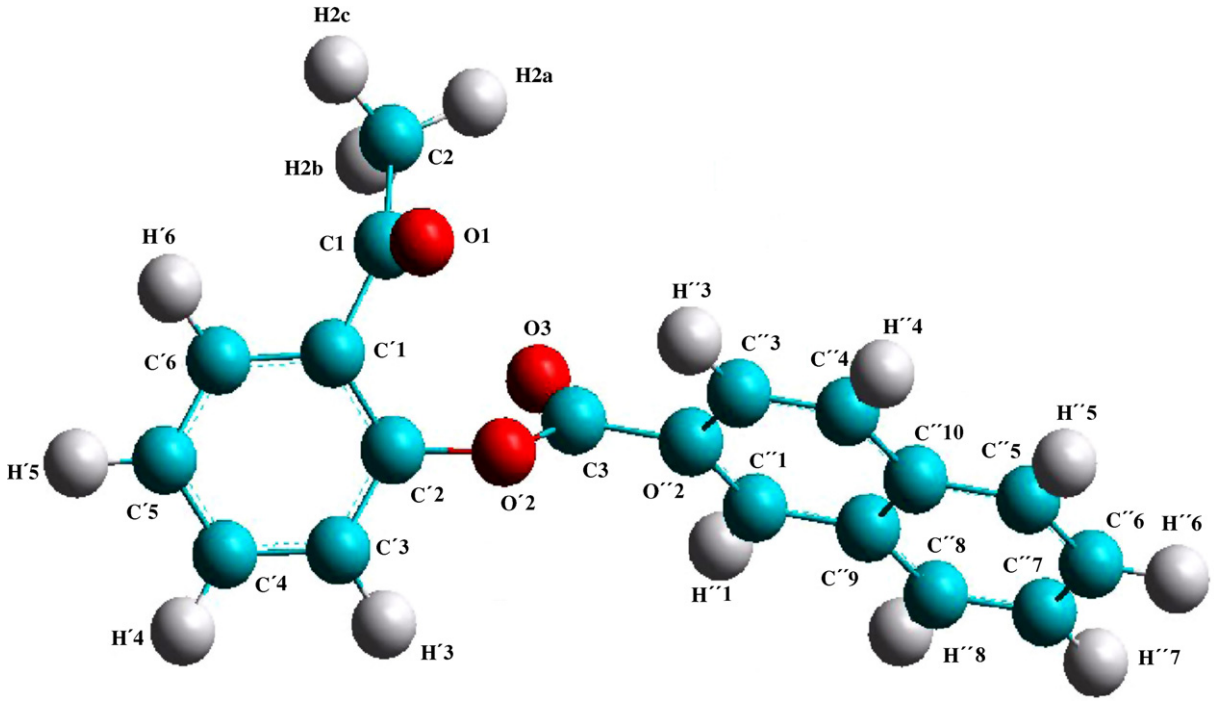

Fig. 1. The lowest energy optimized conformer of 2-acetylphenyl-2-naphthoate calculated at B3LYP/6-31G** level.

2. Experimental

2.1. Chemicals and equipments

2-Acetylphenyl-2-naphthoate: *o*-hydroxyacetophenone (10 mmol), prepared *via* Fries rearrangement from phenol, was placed in a flask and then 2-naphthoyl chloride (12.5 mmol) and 1.0 ml of dry pyridine was added (see Scheme 1). The reaction mixture was stirred for 60 min at room temperature under dry nitrogen carrier. The mixture was poured with stirring into 50 ml of 1 M hydrochloric acid containing 15 g of crushed ice. A white solid was filtered off with suction and washed twice thoroughly with cold water. The crude product was recrystallised from methanol [9,10].

Infrared absorption spectra at 300 and 77 K of 1 cm diameter pellets, made of the 2-acetylphenyl-2-naphthoate microcrystals diluted in spectroscopic grade CsI or polyethylene were recorded with a Bruker FTIR 113v interferometer in the 70–4000 cm^{-1} frequency range at 1 cm^{-1} resolution. The samples were mounted on the cold finger of an Oxford DN 1754 cryostat.

Raman spectra, using a Nd-YAG laser as exciting source, were obtained from pure powders at 300 and 30 K in a backscattering configuration using a Bruker 66 FTIR Raman accessory with the sample mounted on the cold finger of a close cycle He refrigerator (DISPLEX).

2.2. Computational details

The conformational space for 2-acetylphenyl-2-naphthoate was studied using the molecular dynamics (MD) module present in the HyperChem package [35]. Simulations were accomplished with the aid of the MM+ force field also available in that package. Both *cis* and *trans* geometries were used as starting geometries for the simulations. Those geometries were heated from 0 to 600 K in 0.1 ps. Then, the temperature was kept constant by coupling the system to a simulated thermal bath with a bath relaxation time of 0.5 ps. The time step for the simulation was 0.5 fs. After an equilibration period of 10 ps, a 500-ps long simulation was started saving the Cartesian coordinates every 10 ps. Those geometries were then optimized to an energy gradient less than 0.001 kcal $(mol Å)^{-1}$ using the MM+ force field.

The lowest energy conformer of the molecule (Fig. 1) obtained according to the above methodology was further studied using the density functional theory as implemented in the Gaussian 98 package [34]. Geometry optimizations were performed using the Becke's three parameters hybrid functional [36] with the Lee–Yang–Parr correlation functional [37], a combination that gives rise to the well-known B3LYP method. The 6-31G** basis set has been used for all the atoms. The vibrational analysis was performed, and compared with the experimental data, at the same level of theory as it was mentioned above for all the optimized geometries. In this way we verify whether they are local minima or saddle points on the potential energy surface of the molecule. The MEPs were calculated with the Gaussian package and their pictures were obtained with the Molekel program [38].

Chemical shifts were calculated at the same level of theory as above, that is B3LYP/6-31G**. Corrections were performed on the calculated values using the appropriate parameters of a reported regression equation [31–33].

Table 1
Relevant internal coordinates of the lowest energy conformer of 2-acetylphenyl-2-naphthoate compared against experimental values of the constitutional isomer[a]

Internal coordinate	Bond lengths (Å)		Internal coordinate	Bond angles (°)		Internal coordinate	Bond torsion angles (°)	
	Experimental	Calculated		Experimental	Calculated		Experimental	Calculated
O1–C1	1.206(4)	1.23	O1–C1–C1′	122.0(3)	120.75	O3–C3–O2′–C2′	8.2(5)	5.7
O3–C3	1.190(4)	1.23	O1–C1–C2	118.1(3)	121.60	C2″–C3–O2′–C2′	−173.3(3)	−174.5
C1–C1′	1.482(4)	1.51	C1′–C1–C2	119.9(3)	117.62	C3–O2′–C2′–C3′	−102.8(3)	−99.2
C1–C2	1.507(4)	1.53	O3–C3–O2′	121.1(3)	119.70	O3–C3–C2″–C1″	7.5(3)	10.2
C3–O2′	1.366(4)	1.37	O3–C3–C2″	126.8(3)	126.57	O2′–C3–C2″–C1″	10.3(4)	11.4
C3–C2″, C3–C1″	1.466(4)	1.49	O2′–C3–C2″	112.1(3)	113.71	O2′–C3–C2″–C3″	−171.0(3)	−169.2
O2′–C2′	1.391(4)	1.37	C3–O2′–C2′	118.0(2)	124.92	C1′–C2′–O2′–C3	83.3(3)	95.6
C1′–C2′	1.375(4)	1.42	C2′–C1′–C6′	116.4(3)	118.09			
C1′–C6′	1.415(4)	1.41	C2′–C1′–C1	123.7(3)	122.97			
C2′–C3′	1.382(4)	1.39	C6′–C1′–C1	120.0(3)	118.92			
C3′–C4′	1.370(4)	1.38	C1′–C2′–C3′	122.5(3)	120.68			
C4′–C5′	1.364(4)	1.37	C1′–C2′–O2′	121.2(3)	120.46			
C5′–C6′	1.388(4)	1.41	C3′–C2′–O2′	116.0(3)	118.60			
C1″–C2″	1.359(4)	1.37	C4′–C3′–C2′	119.0(3)	119.69			
C1″–C9″	1.424(4)	1.44	C5′–C4′–C3′	121.8(3)	120.18			
C2″–C3″	1.402(4)	1.41	C4′–C5′–C6′	118.4(3)	120.09			
C3″–C4″	1.376(4)	1.38	C5′–C6′–C1′	121.9(3)	121.24			
C4″–C10″	1.387(4)	1.40	C2″–C1″–C9″	121.0(3)	121.42			
C5″–C6″	1.344(6)	1.37	C1″–C2″–C3″	120.3(3)	119.17			
C5″–C10″	1.428(5)	1.43	C1″–C2″–C3	121.5(3)	120.02			
C6″–C7″	1.392(6)	1.41	C3″–C2″–C3	118.2(3)	120.80			
C7″–C8″	1.361(4)	1.38	C4″–C3″–C2″	119.1(3)	120.57			
C8″–C9″	1.400(4)	1.43	C3″–C4″–C10″	122.1(4)	121.32			
C9″–C10″	1.403(4)	1.43	C6″–C5″–C10″	119.5(5)	120.86			
			C5″–C6″–C7″	121.9(4)	120.31			
			C8″–C7″–C6″	119.8(4)	120.23			
			C7″–C8″–C9″	120.6(4)	120.90			
			C8″–C9″–C10″	119.5(3)	118.82			
			C8″–C9″–C1″	122.1(3)	122.13			
			C10″–C9″–C1″	118.4(3)	119.03			
			C4″–C10″–C9″	119.1(3)	118.48			
			C4″–C10″–C5″	122.1(4)	122.65			
			C9″–C10″–C5″	118.8(4)	118.86			

Experimental and calculated bond lengths and bond angles in Å and °, respectively.
[a] From [13].

Table 2
Assignment of the vibrational modes of the IR and Raman spectra of 2-acetylphenyl-2-naphthoate

Theoretical frequencies (cm^{-1})	Experimental frequencies (cm^{-1})				Assignment
	IR		Raman		
	300 K	77 K	300 K	25 K	
18					τC7C1C9H11
22					τC1C7C9H12, H15CC5C6O14
38					τO18C17O14C16, τC6C1C7O8
52					τC2″C3O2′C2′
81	73	73	78	78	τO1C1C1′C2′
104				102	τO1C3C2″C1″, τC2C1C1′C6′
119				113	τH6′C6′C1′C1, τO1C1C1′C6′
158			141	133	τC2″C3O2′C2′
			154sh	147	
				157	
185				173	τC2H2aH2bH2c
187	190	190			Out of plane deformation of the naphtalenic ring τC2H2aH2bH2c
210	202	202	**215**	**219**	τC1″C2″C3O3, τO3C3O2′C2′
234					τO1C1C1′C6′
256	258	258	**261**	**259**, **264**	Out of plane deformation of the naphtalenic ring, τC2″C3O2′C2′, τO1C1C1′C2′
279	273	273	277	277	Out of plane deformation of the benzenic ring τO3C3O2′C2′
346	328	328	332	332	τC1′C1C2H2a
353	348	348			In plane deformation of the naphtalenic ring, τC1″C2″C3O3
402	405	405, 408	**394**	**396**	Out of plane deformation of the naphtalenic ring
416					Out of plane deformation of the benzenic ring, τO1C1C1′C2′
436	433	433	432, 446	432, 446	Out of plane deformation of the benzenic ring, rocking C2H2a-2c
469	455	455	451	451	In plane deformation of the naphtalenic and benzenic ring
485	472, 477, 489	472, 477, 489			Out of plane deformation of the naphtalenic ring
497	**491**	**493**			Out of plane deformation of the naphtalenic ring
514	517	517	518	519	Out of plane deformation of the naphtalenic ring, in plane deformation of the benzenic ring, rocking C2H2a-2c
521					Out of plane deformation of the benzenic ring, in plane deformation of the naphtalenic ring, δC2′O2′C3
526	530	531	533	532	In plane deformation of the naphtalenic ring
575	571	571	570	571	In plane deformation of the naphtalenic and benzenic ring, δC2″C3O3
604	594, 602	594, 603			Out of plane deformation of the benzenic ring, rocking C2H2a-2c
613			612	612	δO1C1C1′, rocking C2H2a-2c, in plane deformation of the benzenic ring
624					Out of plane deformation of the naphtalenic ring, in plane deformation of the benzenic ring
629			638	639	τO3C3O2′C2′, out of plane deformation of the naphtalenic ring
653					In plane deformation of the naphtalenic ring
716			**705**	**707**	In plane deformation of the benzenic ring
729	726	727	729	729	Out of plane deformation of the naphtalenic ring
733					Out of plane deformation of the benzenic ring
770	**765**	**767**, **768**	766	767	Out of plane CH bending C6′H6′(+), C5′H5′(+), C4′H4′(+)
775	776	777			Out of plane CH bending C5″H5″(+), C6″H6″(+), C7″H7″(+), C8″H8″(+)
783	**779**	**782**			In plane deformation of the naphtalenic ring
785	800	800			Out of plane deformation of the naphtalenic ring
815	**831**	**833**			In plane deformation of the naphtalenic and benzenic rings
839	**838**	**840**	**839**	**842**	Out of plane CH bending C3″H3″(+), C7″H7″(+), C8″H8″(+), C1″H1″(−), C5″H5″(−), C24C25H29H31(−)
846	868	869			In plane deformation of the benzenic ring, out of plane CH bending C6′H6′(+), C5′H5′(+)

884	882	883			Out of plane CH bending, C7″H7″(+), C8″H8″(+), C5″H5″(−), C6″H6″(−), C1″H1″(−), C3″H3″(−), C4″H4″(−)
889	894	895			Out of plane CH bending C6′H6′(+), C5′H5′(+), C4′H4′(−), C3′H3′(−)
906	918, 920	919, 921			In plane deformation of the naphtalenic ring, out of plane CH bending, C6′H6′(−), C4′H4′(+), C3′H3′(+)
944	952	953	936	936	Out of plane CH bending, C4′H4′(+), C7″H7″(−), C6″H6″(−), C8″H8″(+), C5″H5″(+)
958	957	957	**952**	**954**	δO1C1C1′, rocking C2H2a-2c, Out of plane CH bending, C6′H6′(−), C3′H3′(−), C5′H5′(+)
962	959	959			Out of plane CH bending, C6′H6′(+), C3′H3′(+), C5′H5′(−), C4′H4(−)
966	964	964	964	965	Out of plane CH bending, C5″H5″(+), C8″H8″(+), C1″H1″(+), C3″H3″(+), C4″H4″(−), C6″H6″(−), C7″H7″(−)
968					In plane deformation of the benzenic and naphtalenic rings, δC2′O2′C3
980					Out of plane CH bending, C3″H3″(−), C4″H4″(−)
995					Out of plane CH bending C6′H6′(+), C4′H4′(+), C5′H5′(−), C3′H3′(−)
997	1014	1015			Out of plane CH bending C6″H6″(+), C8″H8″(+), C5″H5″(−), C7″H7″(−)
1045	1040	1041	**1023**, **1039**	**1025**, **1041**	Rocking C2H2a-2c
1048					In plane CH bending C5″H5″, C6″H6″, C7″H77, C8″H8″, υC6″C7″
1065	1073	1073			In plane C1′C6′ stretching, in plane C6′H6′, C3′H3′, C4′H4′ bending
1090	**1079**	**1081**			In plane C1′C6′ stretching, rocking C2H2a-2c
1098					Deformation and in plane CH bending of the benzenic and naphtalenic rings, rocking C2H2a-2c
1152	1127, 1130	1127, 1130	1130, **1146**	1130, **1149**	CH bending of the benzenic ring
1160	1167	1168	**1167**	**1169**	CH bending of the naphtalenic ring
1180					CH bending of the naphtalenic ring
1185			**1187**	**1189**	In plane CH bending of the naphtalenic ring
1191	1190	1191			In plane CH bending of the benzenic ring
1213	**1206**	**1208**	**1205**	**1208**	In plane CH bending of the naphtalenic ring, δ O3C3C2′
1242					υC3O3, in plane deformation and in plane CH bending of the benzenic and naphtalenic rings
1255	1254	1255	1254	1255	In plane deformation and in plane CH bending of the benzenic and naphtalenic rings
1273	**1262**, **1271**, **1275**	**1264**, **1273**, **1277**	**1271**	**1274**	In plane deformation and in plane CH bending of the benzenic and naphtalenic rings, rocking C2H2a-2c, υC1′C1
1292		1281			In plane CH bending of the naphtalenic ring
1296					In plane CH bending of the naphtalenic and benzenic rings and stretching of the naphtalenic ring
1303	1304	1305	1304	1305	In plane CH bending of the benzenic ring
1353	1359	1358			Stretching of the benzenic ring and In plane CH bending of the benzenic ring
1391	1389	1389	1377, **1388**	1378, **1390**	Stretching of the naphtalenic ring and in plane CH bending
1395					Asymmetric δC2H2a-2c
1412	1417	1417			Stretching of the naphtalenic ring and In plane CH bending
1425	1439, **1449**	1439, **1451**	**1438**	**1440**	Stretching of the naphtalenic ring and In plane CH bending
1480	1485	1486	**1468**	**1472**	Stretching of the naphtalenic ring and In plane CH bending
1482	1485	1485	**1478**	**1482**	Asymmetric δC2H2a-2c
1489					Symmetric δC2H2a-2c, stretching of the benzenic ring and in plane CH bending
1494					Asymmetric δC2H2a-2c
1511	1508	1509			Stretching of the naphtalenic ring and in plane CH bending
1521	1519	1519			Stretching of the naphtalenic ring and in plane CH bending
1558	1555	1555	**1577**	**1579**	Stretching of the naphtalenic ring and in plane CH bending
1623	1605	1602, 1606	1593, 1600, **1605**	**1607**	Stretching of the naphtalenic ring and in plane CH bending
1626	1629	1630	**1629**	**1631**	Stretching of the benzenic ring and in plane CH bending
1656	1650	1650			Stretching of the naphtalenic and benzenic rings and in plane CH bending
1660					Stretching of the benzenic ring and In plane CH bending
1684	1691	1692	**1690**	**1692**	Stretching of the naphtalenic ring and In plane CH bending

Table 2 (*continued*)

Theoretical frequencies (cm^{-1})	Experimental frequencies (cm^{-1})						Assignment
	IR			Raman			
	300 K	77 K		300 K	25 K		
1775		1731	1730		1731	1730	νC1O1
1824							νC3O3
2837		2852	2849, 2857				Symmetric stretching C2H2a-2c
2897		2872					Asymmetric stretching C2H2a-2c
2947		2913, **2921**	**2917**		**2920**	**2916**	Asymmetric stretching C2H2a-2c
2954							Stretching C6′H8″, C6′H6″, C5″H5″
2959							Stretching C4′H4″↑, C7″H7″↓, C8″H8″↓
2961						2969	Stretching C3′H3″↑, C7″H7″↑, C6″H7″↑, C4′H4″↓C8″H8″↓C5″H5″↓
2967		2968	2968				Stretching C5′H5′↓, C4′H4′↓
2970							Stretching C7′H7″↓, C8″H8″↓, C5″H5″↓, C6″H6″↓
2980							Stretching C5′H5′↓, C4′H4′↓, C6′H6′↓, C3′H3′↓
2981							Stretching C6′H6″↓, C7″H7″↓, C1″H1″↑
2983					2984	2984	Stretching C1″H1″↑, C8″H8″↑, C7″H7″↑
2992							Stretching C4′H4′↓, C3′H3′↓, C6′H6′↑
2998		3001	3001			3001	Stretching C6′H6′↑, C5′H5′↑, C4′H4′↑
3025	3032, 3039, 3067, 3073, 3077, **3081**		3029, 3032, 3039, 3067, 3077, **3083**	3061, 3066, 3084, 3089	3061, 3065, 3078, 3086, 3096		Stretching C3′H3″↑

Bold wavenumbers correspond to those show shifting when the temperature is lowered. ↓ and ↑ correspond to stretching in plane movements in and out of the corresponding ring.

3. Results and discussion

3.1. Optimized geometrical parameters and energy of the lowest energy conformers of 2-acetylphenyl-2-naphthoate

The lowest energy optimized conformer of 2-acetylphenyl-2-naphthoate calculated at B3LYP/6-31G** level is shown in Fig. 1.

Table 1 summarizes the relevant internal coordinates of 2-acetylphenyl-2-naphthoate lowest energy conformer. They are compared against experimental crystallographic data values of the 2-acetylphenyl-1-naphthoate [13] showing a good agreement in bond lengths and bond angles. The difference to be remarked corresponds to the dihedral angles since in the 2-acetylphenyl-1-naphthoate the dihedral angle between the planes corresponding to the benzene and the naphthalene rings is 77.39 while in the 2-acetylphenyl-2-naphthoate is −174.5, nearly in the same plane as it would be expected.

3.2. Raman and IR spectra

Table 2 shows the calculated and assigned frequencies of modes active in infrared and Raman for 2-acetylphenyl-2-naphthoate, at room and low temperatures. As it was pointed out above the vibrational modes assignments were performed by visualization on the corresponding animation by means of the Molekel computational codes [38]. The reported theoretical values correspond to the conformer of lowest energy. Nevertheless calculations were performed over *cis* and *trans* structures and can be provided under request.

The overall infrared (IR) and Raman spectra of 2-acetylphenyl-2-naphthoate at 300 and 77 and 25 K are shown in Fig. 2. These spectra show softening ($\Delta = -$) and hardening ($\Delta = +$) of several vibrational modes implying subtle local structural changes in the molecule as it cools down, Fig. 2(a–l). Frequency shifting of $\Delta = 2; 3; -3\ cm^{-1}$ is seen in the IR spectrum (Fig. 2(a–c, g–i)).

Frequency shifting of $\Delta = 2; 3; -4\ cm^{-1}$ is found in the Raman spectrum (Fig. 2(d–f, j–l)).

In the IR spectra hardening is observed on the bands located at: 491, 765, 831, 838, 1079, 1206, 1262, 1271, 1275, 1449, 3081 and 779 cm^{-1}, respectively. Softening is localized in the corresponding mode at 2921 cm^{-1}. Assignments of all vibrational modes of the IR and Raman spectra of 2-acetylphenyl-2-naphthoate are collected in Table 2.

It is worth mentioning that an inspection of the IR spectra in the regions around 1690–1731 cm^{-1} corresponding to the absorption of the stretching νC1O1 and νC3O3 shows that the features do not undergo further splitting as the temperature is lowered indicating the existence of a single conformation in the interval of temperature studied.

3.3. Molecular electrostatic potential maps

As we stated above, the electrostatic potential has been used primarily for predicting sites, relative reactivities towards electrophilic attack, in biological recognition and hydrogen bonding interactions [19–22]. The emphasis of these studies has been on negative regions of $V(r)$. In the majority of the potential electrostatic maps the regions of negative values account for the local minima and are site candidates of electrophilic attack. The positive regions have maxima only in the nuclear positions [39] indicating that there are no affinities by nucleophilic reactives.

The molecular electrostatic potential of the most stable conformer of 2-acetylphenyl-2-naphthoate depicted in Fig. 3 shows that it has several possible sites for electrophilic attack in which

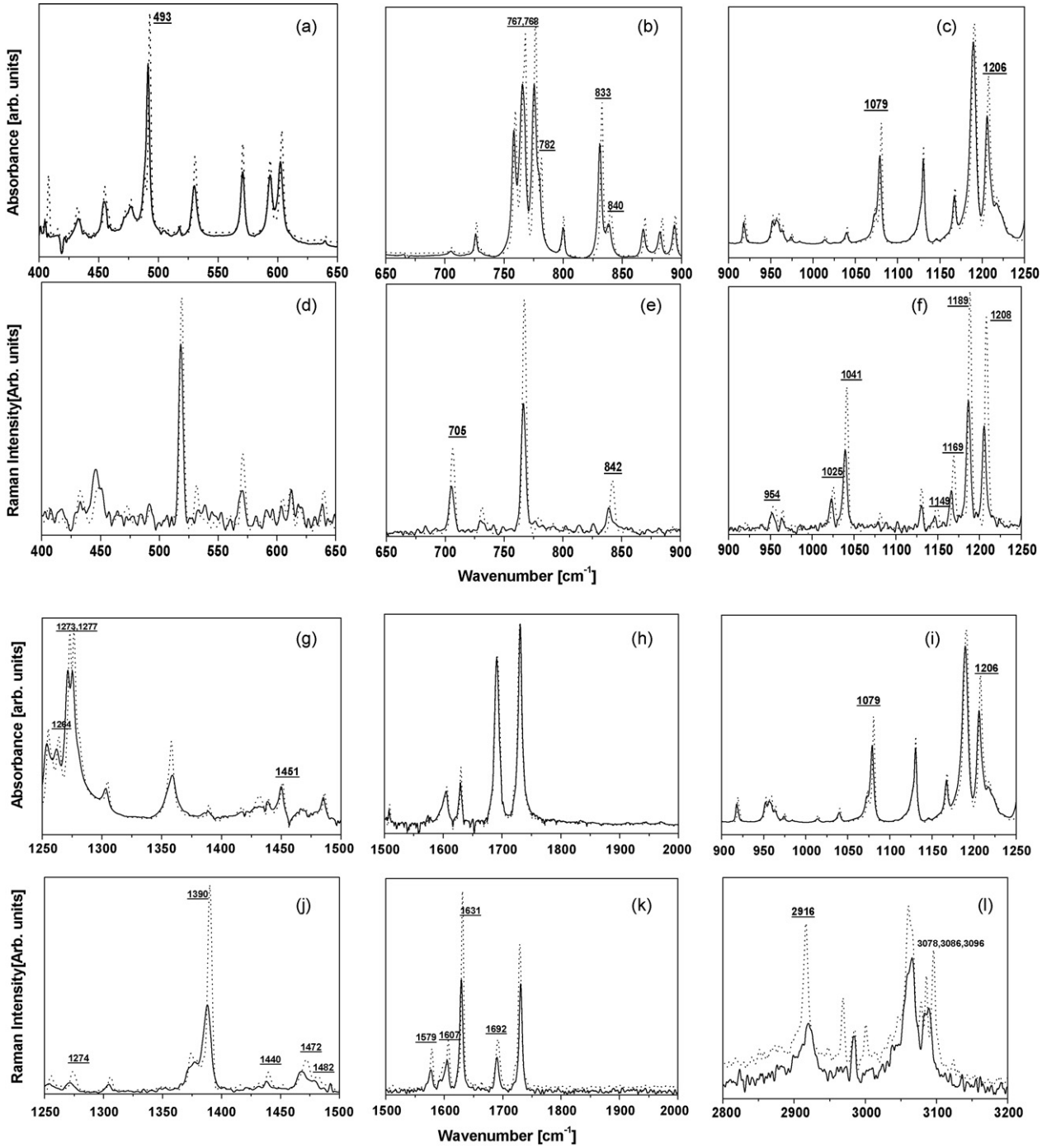

Fig. 2. IR and Raman spectra of 2-acetylphenyl-2-naphthoate. IR and Raman spectra at 300 K (full line) and 77 K (dotted line) and 300 K (full line) and 25 K (dotted line), respectively, between 400 and 4000 cm^{-1}; (a–f) shows the spectra details between 400 and 1260 cm^{-1} and (g–l) accounts for the IR and Raman spectra between 1200 and 3200 cm^{-1}.

$V(r)$ calculations provide insights into the order of preference in addition to the calculated 3D electrostatic potential contour map of 2-acetylphenyl-2-naphthoate. Negative regions are associated with O_{1-3} with values around −0.10302, −0.08103 and −0.09569 a.u., respectively. Thus, it would be predicted that the O_1, O_2 and O_3 atoms will be the preferred sites for the electrophilic attack. Positive regions are localized on the hydrogen atoms with a value around +0.04361 a.u. and up and down of the center of the rings and on the C2″ atom indicating possible sites for nucleophilic attack.

3.4. NMR spectra

Experimental and *ab initio* values of the NMR chemical shifts of 2-acetylphenyl-2-naphthoate are collected in Table 3 together with the corrected values due to the application of the regression formulae for *ab initio* and density functional chemical shifts developed by van Eikema Hommes and Clark [33]. The corrected values show better approximation to the experimental ones especially for the carbon atoms, whereas the hydrogen atoms have not substantial improvement. Besides, the calculated data pre-

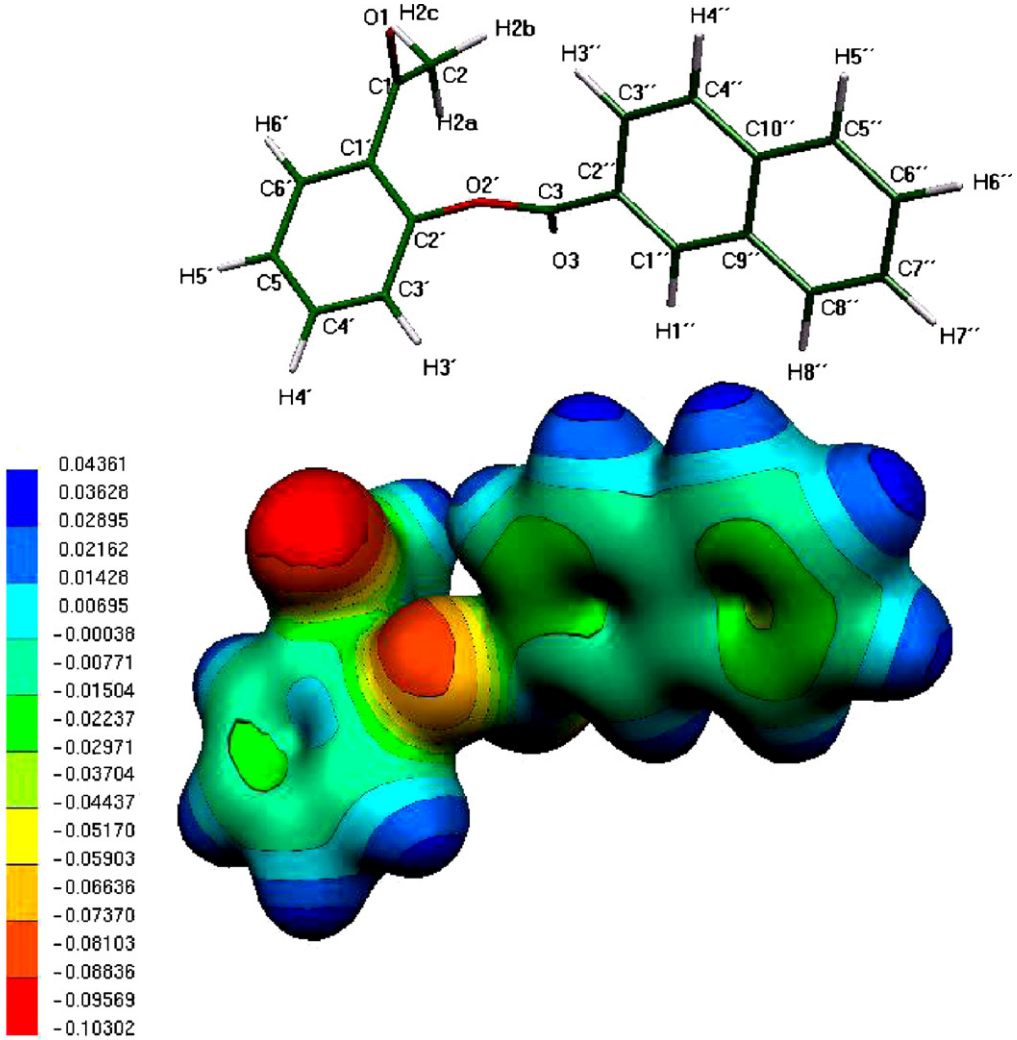

Fig. 3. Map of the molecular electronic potential (MEP) for 2-acetylphenyl-2-naphthoate, in a.u.

Table 3
Experimental[a] and calculated[b] NMR chemical shifts and corrected values[c] of 2-acetylphenyl-2-naphthoate

Atom	Experimental chemical shifts[a]	Theoretical chemical shifts[b]	Corrected values[c]
C1	197.5	193.92	196.09
C2	29.8	33.80	24.53
C3	165.3	165.20	165.32
C1′	131.4	128.55	128.36
C2′	149.5	156.14	155.62
C3′	124.0	127.31	124.72
C4′	133.4	134.50	132.43
C5′	126.2	125.82	123.13
C6′	130.3	133.70	131.57
O1	579	617.36	
O2′	188	215.86	
O3	347	370.39	
C1″	132.2	136.28	134.65
C2″	126.2	130.93	128.20
C3‴	125.4	128.73	126.25
C4″	128.6	129.56	127.13
C5″	127.8	129.61	127.18
C6″	128.7	129.17	126.72
C7″	126.9	127.31	124.72
C8″	129.6	132.01	129.75
C9″	132.5	134.24	132.15
C10″	135.9	137.06	135.17
H2a	2.56	2.16	2.34
H2b	2.56	3.03	3.21

Table 3 (*Continued*)

Atom	Experimental chemical shifts[a]	Theoretical chemical shifts[b]	Corrected values[c]
H2c	2.56	2.97	3.15
H3′	7.28	7.63	7.84
H4′	7.37	7.93	7.76
H5′	7.37	7.71	7.92
H6′	7.87	8.30	8.51
H1″	8.80	9.23	9.38
H3″	8.19	8.82	8.67
H4″	7.95	8.19	8.33
H5″	7.91	8.22	8.36
H6″	7.99	8.02	8.08
H7″	7.57	7.94	7.30
H8″	7.99	8.37	8.21

Numbers refer to those in Fig. 1.

[a] Experimental chemical shifts taken from Ref. [11]. Values given in δ (ppm). Relative to TMS and $CDCl_3$ as solvent for ^1H and ^{13}C and relative to H_2O as external reference and acetonitrile as solvent for ^{17}O.

[b] Theoretical chemical shifts calculated at B3LYP/6-31G(d) level.

[c] Corrected values given by the regression equations from Ref. [33]. ^1H: $\kappa = -1.0065$, $\delta = 32.46$; ^{13}C: $\kappa = -1.0715$; $\delta = 200.65$. Regression equation $\delta = \delta^0 + \kappa\sigma$.

dict the same chemical shift sequence for the hydrogen atoms H-6″ and H-7″ than those found experimentally in compounds with 2-naphthyl substituents [11], showing that the mesomeric effects should be considered as a relevant feature to solve chemical shift assignments. Calculated ^{17}O chemical shifts show the similar order than the experimental ones and allow unambiguous assignment of all signals, but the predicted values are strikingly more positive than the experimental ones (from 23 to 38 ppm). The last feature exhibits the sensitivity of the ^{17}O chemical shift values reflecting the electronic changes due to conformation [14]. The preferred conformation in gas phase could be modified in condensed phase since the solvent intramolecular interaction exerts protective influence shifting the experimental data to higher fields.

4. Conclusions

We have studied the mid-, far-infrared and Raman spectra of 2-acetylphenyl-2-naphthoate at room and low temperatures in the 60–4000 cm^{-1} spectral range. They show several bands whose frequency positions shift towards high- and low-wavenumbers when the temperature is lowered, indicating molecular bond stiffening or weakening to the existence of intra- and intermolecular interactions reflecting subtle changes in their local structure as the temperature change accordingly.

The lowest energy conformers of 2-acetylphenyl-2-naphthoate, studied using the density functional theory at B3LYP/6-31G** level correspond to a geometry similar to the 2-acetylphenyl-1-naphthoate except that the planes that contains the benzene and the naphthalene rings are nearly coplanar.

From the calculation it can be seen that the energies of the different conformers corresponding to geometries where different torsion angles were varied are in a range of 25 kcal, being the lowest one the rotamer shown in Fig. 1.

We also deduced from the experimental IR data, by inspection of the C=O stretching band, the existence of a single conformer from 300 to 77 K.

The molecular electrostatic potential of 2-acetylphenyl-2-naphthoate shows that this molecule has several possible sites for electrophilic attack in which $V(r)$ calculations provide insights into the order of preference. Negative regions are associated with O_1, O_2 and O_3. Thus, it is predicted that the oxygen atoms will be the preferred electrophilic sites. Positive regions are localized on the hydrogen atoms with a value around +0.04361 a.u. and up and down of the center of the rings and on the C2′ atom indicating possible sites for nucleophilic attack.

Experimental and *ab initio* calculated values of the NMR chemical shifts of 2-acetylphenyl-2-naphthoate show a good fitting and the last one allows us to predict ^{17}O NMR chemical shifts.

Acknowledgments

The authors acknowledge CONICET, Universidad Nacional de La Plata and Universidad de Buenos Aires (Argentina) for financial support. A.H.J. is member of the Scientific Research Career (CIC, Provincia de Buenos Aires), Argentina. N.E.M. is pleased to acknowledge financial support from the Consejo Nacional de Investigaciones Científicas y Técnicas (CONICET) under project: PIP 5152.

References

[1] G. Atassi, P. Biret, J.J. Berthelon, F. Collonges, Eur. J. Med. Chem. Ther. 20 (1985) 343.
[2] P. Biret, J.J. Berthelon, F. Collonges, Fr. Demande, FR 2,536,397 (1984) (Appl. 82 (1982) 19640).
[3] Y.B. Vibhute, J. Indian Chem. Soc. 53 (1976) 736.
[4] G.R. Subbanwad, Y.B. Vibhute, J. Indian Chem. Soc. 69 (1992) 337.
[5] R.T. Buckler, O.L. Garling, F.E. Ward, U.S., US 4,241,069 (1980) (Appl. 72 (1979) 105).
[6] Y.B. Vibhute, S.A. Wadje, Indian J. Exp. Biol. 14 (1976) 739.
[7] S.V. Kuberkar, Y.B. Vibhute, Asian J. Chem. 4 (1992) 22.
[8] G.R. Subbanwad, Y.B. Vibhute, M.S. Shingare, J. Indian Chem. Soc. 68 (1991) 570.
[9] J.L. Jios, J.C. Autino, A.B. Pomilio, An. Asoc. Quim. Argent. 83 (1995) 183.
[10] J.L. Jios, Doctoral Thesis, Universidad Nacional de La Plata, 1996.
[11] J.L. Jios, H. Duddeck, Z. Naturforsch. 55b (2000) 189.
[12] G.P. Romanelli, J.L. Jios, J.C. Autino, L.F.R. Cafferata, D. Ruiz, E.A. Castro, Chem. Anal. (Warsaw) 47 (2002) 205.
[13] A.E. Goeta, G. Punte, J.L. Jios, J.C. Autino, Acta Crystallogr. C 52 (1996) 2045.
[14] (a) D.W. Boykin (Ed.), ^{17}O NMR Spectroscopy in Organic Chemistry, CRC Press Uniscience, Boca Raton, FL, 1991;
(b) S. Berger, S. Braun, H.-O. Kalinowski, NMR-Spektroskopie von Nichtmetallen, Band 1, Thieme, Stuttgart, New York, 1992.
[15] C. Muñoz-Caro, A. Niño, M.L. Sement, J.M. Leal, S. Ibeas, J. Org. Chem. 65 (2000) 405.
[16] P. Politzer, P.R. Laurence, K. Jayasuriya, in: J. McKinney, Structure Activity Correlation in Mechanism Studies and Predictive Toxicology, Special Issue of Environ. Health Perspect. 61 (1985) 191.
[17] P. Politzer, J.S. Murray, in: D.L. Protein, R. Beveridge, Lavery (Eds.), Theoretical Biochemistry and Molecular Biophysics: A Comprehensive Survey, vol. 2, Adenine Press, Schenectady, NY, 1991, (Chapter 13).
[18] P. Politzer, D.G. Truhlar (Eds.), Chemical Applications of Atomic and Molecular Electrostatic Potentials, Plenum Press, NY, 1981.
[19] P. Politzer, S.J. Landry, T. Warnheim, Phys. Chem. 86 (1982) 4767.
[20] P. Politzer, L. Abrahmsen, P. Sjoberg, J. Am. Chem. Soc. 106 (1984) 85.
[21] P. Politzer, P.R. Laurence, L. Abrahmsen, B.A. Zilles, P. Sjoberg, Chem. Phys. Lett. 111 (1984) 75.
[22] J.S. Murray, P. Lane, T. Brinck, P. Politzer, P. Sjoberg, J. Phys. Chem. 95 (1991) 14.
[23] R.F.W. Bader, Chem. Rev. 91 (1990) 893.
[24] R. Ditchfield, D.P. Miller, J.A. Pople, Chem. Phys. Lett. 6 (1970) 573.
[25] U. Gelius, B. Roos, P. Siegbahn, Chem. Phys. Lett. 4 (1970) 471.
[26] R. Ditchfield, Chem. Phys. Lett. 15 (1972) 203.
[27] M. Kaupp, V.G. Malkin, O.L. Malkina, D.R. Salahub, Chem. Eur. J. 2 (1996) 24.

[28] M. Schindler, W. Kutzelnigg, J. Am. Chem. Soc. 105 (1983) 1360.
[29] J. Gauss, J. Chem. Phys. 99 (1993) 3629.
[30] C.J. van Wüllen, Chem. Phys. 102 (1995) 2806.
[31] Chesnut, in: L.B. Lipkowitz, D.B. Boyd (Eds.), Reviews in Computational chemistry, vol. 8, VCH, NY, 1996, (Chapter 5).
[32] D.A. Forsyth, A.B. Sebag, J. Am. Chem. Soc. 119 (1997) 9483.
[33] N.J.R. van Eikema Hommes, T. Clark, J. Mol. Model. 11 (2005) 175.
[34] M.J. Frisch, G.W. Trucks, H.B. Schlegel, G.E. Scuseria, M.A. Robb, J.R. Cheeseman, V.G. Zakrzewski, J.A. Montgomery Jr., R.E. Stratmann, J.C. Burant, S. Dapprich, J.M. Millam, A.D. Daniels, K.N. Kudin, M.C. Strain, O. Farkas, J. Tomasi, V. Barone, M. Cossi, R. Cammi, B. Mennucci, C. Pomelli, C. Adamo, S. Clifford, J. Ochterski, G.A. Petersson, P.Y. Ayala, Q. Cui, K. Morokuma, D.K. Malick, A.D. Rabuck, K. Raghavachari, J.B. Foresman, J. Cioslowski, J.V. Ortiz, A.G. Baboul, B.B. Stefanov, G. Liu, A. Liashenko, P. Piskorz, I. Komaromi, R. Gomperts, R.L. Martin, D.J. Fox, T. Keith, M.A. Al-Laham, C.Y. Peng, A. Nanayakkara, C. Gonzalez, M. Challacombe, P.M.W. Gill, B. Johnson, W. Chen, M.W. Wong, J.L. Andres, C. Gonzalez, M. Head-Gordon, E.S. Replogle, J.A. Pople, Gaussian 98, Revision A.7, Gaussian Inc., Pittsburgh, PA, 1998.
[35] HyperChem Release 7.5, Hypercube Inc., USA.
[36] A.D. Becke, J. Chem. Phys. 98 (1993) 5648.
[37] C. Lee, W. Yang, R.G. Parr, Phys. Rev. B 37 (1988) 785.
[38] P. Flúkiger, H.P. Lúthi, S. Portmann, J. Weber, MOLEKEL 4.0, Swiss Center for Scientific Computing, Manno, Switzerland, 2000.
[39] K. Pathak, S.R. Godre, J. Chem. Phys. 93 (1990) 1770.